Coupling effects of native H_2S and different co-injected impurities on CO_2 sequestration in layered saline aquifers

Didi Li[1], Xi Jiang[2*], Yuhui Zhong[1], Aihua Liu[1]*

[1] *Guangzhou Key Laboratory of Environmental Catalysis and Pollution Control, School of Environmental Science and Engineering, Institute of Environmental Health and Pollution Control, Guangdong University of Technology, Guangzhou 510006, China*

[2] *School of Engineering and Materials Science, Queen Mary University of London, Mile End Road, London E1 4NS, UK*

[*] *Corresponding authors: Didi Li (ddli@gdut.edu.cn); Xi Jiang (xi.jiang@qmul.ac.uk)*

Abstract

Impurity effects are an intricate issue in CO_2 geological storage, involving both pre-dissolved impurities in the geological medium and co-injected impurities. Numerical simulations were carried out in this study to investigate the coupling effects of pre-dissolved H_2S and different co-injected impurities (H_2S, CH_4 and N_2) on CO_2 sequestration in layered sour saline aquifers. The native H_2S would be exsolved out of the sour formation brine and pushed ahead by the injected plume. The exsolved H_2S reduced the concentrations of the injected gases at the two-phase interface. Particularly, when H_2S was co-injected with CO_2 into the sour saline aquifers, both dissolved CO_2 inventory and dissolved CO_2 ratio would reduce by nearly half compared with that in the regular saline aquifers without native H_2S. It was observed that the decrease of the dissolved CO_2 ratio due to the existence of the native H_2S is much compensated by the co-injection of CH_4 or N_2. Nevertheless, the native impurity seems to have more profound effects on CO_2 sequestration than the co-injected impurities. The results should be considered in selecting appropriate sequestration sites and establishing risk assessment strategies.

Keywords: CO_2 geological sequestration, native H_2S, co-injected impurity, numerical simulation

1. Introduction

CO_2 geological storage (CGS) is one of the promising options to reduce CO_2 emissions from power plants based on fossil fuels (mainly natural gas and coal) into the atmosphere (Bachu 2008, Jiang 2011). Furthermore, CGS is regarded as the only available technology that addresses this greenhouse gas issue while allowing for the continued use of fossil fuels (Celia 2017, Oh et al. 2019). There are different candidate reservoirs for CGS, including deep saline aquifers, depleted oil and gas reservoirs, and unminable coal beds (Aminu et al. 2017). Amongst them, CGS in the deep saline aquifers is expected to be the most promising option in the short-to-medium term (Jiang 2011). While non-CO_2 species could be commonly included in the injected CO_2 streams in order to reduce the total cost of CGS, they could also be found within the formation reservoir prior to CO_2 injection. It has been proven that some potential deep saline aquifers suitable for CO_2 geological storage may contain a combination of dissolved CO_2, H_2S and/or light hydrocarbons such as methane (Ghaderi et al. 2011a, b, Talman 2015). For example, the Nisku aquifer in Canada which is designated for large-volume CO_2 injection and storage contains certain concentration of dissolved H_2S (Hutcheon 1999).

Similar to the co-injected impurities, these pre-existing species are expected to affect the transport and long-term fate of the injected CO_2 streams and certainly are worthy of attention. However, the impurity effects on CGS are intricate and have not been fully understood. In fact, the available investigations mainly focused on pure CO_2 injection in to reservoirs containing pre-dissolved CH_4 or H_2S. Both field observations and simulation results suggested that the pre-existing species would exsolve out of the formation brine in response to CO_2 injection (Battistelli and Marcolini 2009, Doughty and Freifeld 2013, Li and Li 2015). For example, it has been confirmed that CO_2 is capable of removing less soluble components such as CH_4 from the formation brine (Qafoku et al. 2017). It was unlikely for the extracted CH_4 to dissolve back into the formation brine (Taggart 2010). Field observations and sampling also confirmed the emergence of an anomalously increased CH_4 concentration near the plugged and abandoned wells (Hovorka et al. 2011). There could be a nearly pure CH_4-rich plume ahead of the CO_2 displacement front (Hosseini et al. 2012,

53 Soltanian et al. 2018). The extraction of native CH_4 and the resulting CH_4 plume ahead of the CO_2
54 plume could be useful in monitoring leakage (Qafoku et al. 2017). The extraction of CH_4 may also
55 provide additional methane mobilization and recovery. In the case of geopressured-geothermal
56 aquifers with large quantities of dissolved methane and geothermal energy, the application of the
57 produced CH_4 along with geothermal energy had the potential to offset the cost of capture and
58 storage (Ganjdanesh et al. 2015). For natural gas reservoirs, injecting CO_2 would result in enhanced
59 gas recovery and effective CO_2 sequestration at the same time (Zangeneh et al. 2013). However,
60 for most potential storage reservoirs, the feasibility of the beneficial use of the produced CH_4 was
61 pretty low because the gas-phase saturations in the CH_4-rich bank were too small (Oldenburg et al.
62 2013).

63 Apart from the low-solubility CH_4, dissolved H_2S in the saline aquifers prior to CO_2 injection
64 was also implied to be extracted from the formation aquifers during gas injection. Since H_2S has a
65 more preferential solubility in the formation brine than CH_4, the amount of H_2S which has the
66 potential to partition into the gas phase was also more significant (Talman 2015). Depending on
67 the thermodynamic equilibrium at the two-phase boundary, it was suggested that there was
68 substantial fraction of H_2S accumulating at the leading edge of the advancing plume during CO_2
69 injection (Ghaderi et al. 2011a, b, Ghaderi and Leonenko 2015). The leading edge of the plume
70 may even contain pure H_2S depending on the reservoir conditions (Cholewinski et al. 2016).

71 The aforementioned investigations play an important role in establishing monitoring strategies
72 as well as risk assessment for potential leakage during CO_2 sequestration, especially for projects in
73 the sour saline aquifers containing toxic H_2S. However, investigations about the interplay of the
74 native impurity and the co-injected impurity on CO_2 sequestration are much lacking, especially for
75 the coupling effects of the pre-dissolved H_2S in saline aquifers and different co-injected impurities.
76 Furthermore, most previous studies investigating the effects of native H_2S on CO_2 sequestration
77 have adopted one-dimensional radial system which was assumed to be homogeneous and isotropic,
78 while most potential geological formations are layered due to deposition and erosion in the strata
79 forming process. In the present study, we evaluate and compare the coupling effects of native H_2S

and different co-injected impurities, including H_2S, N_2, and CH_4, on CO_2 sequestration in layered saline aquifers. Our goal is to provide insights on the transport and fate of both co-injected and pre-existing impurities in more realistic layered reservoirs, which might be helpful in the deployment of large-scale CGS technology.

2. Simulation methodology

2.1 Model setup

Numerical simulations are performed in the layered formation with alternating high-permeability (as well as high-porosity) and low-permeability (as well as low-porosity) layers to simply mimic real reservoirs in a realistic way. As shown in Figure 1, the present model is mainly patterned after the Sleipner project in the Utsira Formation (Pruess et al. 2002). The two-dimensional (2D) vertical section is 184 m in height and 6000 m in length. The width of the 2D section is one-meter thick. The adopted model embeds four layers of low-permeability shale in the high-permeability sand to represent the main features of the host formation. For simple reference, the four shale layers are naming as SL1 to SL4 from top to bottom. The injection well which is represented by IP (injection point) for simplicity, is 30 m below SL4 and 22 m above the bottom boundary. The left boundary condition is set as no flux while the right boundary 6000 m away is set to have constant hydrostatic pressure in order to prevent potential overpressure. Both the top and bottom boundaries are set as impermeable.

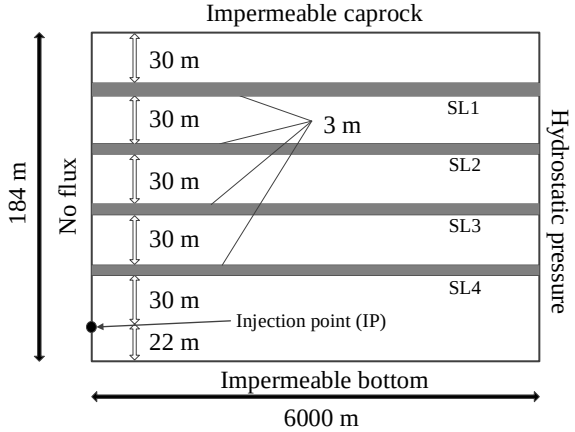

Figure 1. Schematic representation of the modelling domain, modified from Pruess et al. (Pruess et al. 2002).

100 Generally, CO_2 sequestration in deep saline aquifers is expected to occur at depths below 800
101 m where CO_2 has a high density ranging from 500-800 kg/m^3, which is beneficial to the storage
102 efficiency and security (Metz et al. 2005). Assuming the injection point in the present model is at
103 depth below 1200 m, the temperature at the injection well is taken as 61 °C, given that the
104 temperature at the land surface is 25 °C and that the geothermal gradient is 30 °C/km. The
105 hydrostatic pressure at depth below 1200 m is assumed to be 110 bar. The details of the formation
106 and fluid properties are listed in Table 1. The salinity and injection rate are the same as those in the
107 investigation of Ghaderi et al. (Ghaderi et al. 2011a), while the values of porosity and permeability
108 for both the sand and shale layers are adopted from a sample problem using similar model (Pruess
109 et al. 2002). All the other properties are taken from our previous investigation of the co-injected
110 impurities in stratified formation (Li et al. 2017, 2018).

111 Table 1. Fluid properties and model parameters.

Property	Value
Temperature at injection well	61 ℃
Pressure at injection well	110 bar
Salinity	118950 mg/L
Sand permeability	3×10^{-12} m^2
Shale permeability	1×10^{-14} m^2
Vertical to horizontal permeability ratio	0.1
Sand porosity	0.35
Shale porosity	0.1025
Residual gas saturation	0.05
Irreducible liquid saturation	0.2
Injection rate	4 m^3/day
Injection time	2 years
Simulation time	10 years

112 It has been suggested that the possible upper limit of the co-injected impurity in most practical
113 CGS projects is 10% (mole fraction) (Li et al. 2011). In the present study, the concentration of all
114 the co-injected impurity in the CO_2 stream is chosen to be 10% to compare the effects of different
115 co-injected impurities in the sour saline aquifers. Five scenarios with different injected
116 compositions and pre-existing H_2S conditions are selected, as listed in Table 2. The first four

117 scenarios are set to investigate the coupling effects of different co-injected impurities and native
118 H_2S while the last scenario is used to evaluate the effects of native H_2S on sour gas (CO_2 and H_2S
119 mixture) injection into the regular saline aquifers. It can be seen that two concentrations are chosen
120 for the pre-dissolved H_2S, *i.e.*, saturated or none at all. In practical, considering the high solubility
121 of H_2S in the formation brine and the tremendous capacity of potential reservoirs, along with the
122 economic and secure concerns, it is unlikely that the sour reservoirs chosen for CO_2 sequestration
123 are saturated with H_2S. In fact, previous investigation suggested that the concentration of dissolved
124 H_2S was only "measurable" rather than "saturated" (Hutcheon 1999). Still, as a preliminary and
125 sensitivity investigation, the case of saturated dissolved H_2S is adopted to obtain understanding of
126 extreme consequences of pre-dissolved H_2S. The density and viscosity of the chosen species under
127 the condition at the injection point are listed in Table 3.

128 Table 2. Injected compositions and pre-exsiting H_2S conditions for different simulation scenarios.

Scenario No.	Scenario name	Injected composition	Pre-existing H_2S
a	Base	100% CO_2	Saturated
b	10% H_2S	90% CO_2 + 10% H_2S	Saturated
c	10% CH_4	90% CO_2 + 10% CH_4	Saturated
d	10% N_2	90% CO_2 + 10% N_2	Saturated
e	10% H_2S without pre-H_2S	90% CO_2 + 10% H_2S	None

129 Table 3. Density and viscosity of different species at the injection point.

Species	Density (kg/m^3)	Viscosity (Pa·s)
CO_2	349.10	2.687×10^{-5}
H_2S	706.59	1.048×10^{-4}
CH_4	70.06	1.473×10^{-5}
N_2	108.14	2.137×10^{-5}

130 *2.2 Modelling approach*

131 The compositional reservoir simulator CMG-GEM (Computer Modelling Group, 2012),

capable of multiphase multicomponent flow simulations, is employed to perform the computational simulations. Assuming local thermodynamic equilibrium of the gaseous and aqueous phase, the general Henry's law (Li and Nghiem, 1986) is used to calculate the dissolution and exsolution of the gas components in and from the formation brine,

$$f_i = x_i H_i \tag{1}$$

where f_i is the fugacity of component i in the gaseous phase, x_i is the mole fraction of component i in the aqueous phase, and H_i is the Henry's constant of component i. The gas fugacity is calculated by the Peng-Robinson equation of state (EOS) (Peng and Robinson 1976) while the Henry's constant at pressure p and temperature T is calculated using the Harvey's correlation (Computer Modelling Group 2012, Harvey 1996),

$$\ln H_i = \ln H_i^s + \frac{1}{RT}\int_{p_{\mathrm{H2O}}^s}^{p} v_i dP \tag{2}$$

$$\ln H_i^s = \ln p_{\mathrm{H2O}}^s + A(T_{r,\mathrm{H2O}})^{-1} + B(1-T_{r,\mathrm{H2O}})^{0.355}(T_{r,\mathrm{H2O}})^{-1} + C[\exp(1-T_{r,\mathrm{H2O}})](T_{r,\mathrm{H2O}})^{-0.41} \tag{3}$$

$$T_{r,\mathrm{H2O}} = \frac{T}{T_{\mathrm{c,H2O}}} \tag{4}$$

where H_i^s is Henry's constant of component i at the saturation pressure of H_2O (p_{H2O}^s) and temperature T, v_i is the partial molar volume of component i in the aqueous phase, $T_{r,\mathrm{H2O}}$ and $T_{c,\mathrm{H2O}}$ is the reduced temperature and critical temperature of H_2O, respectively. For the selected gas components in the present study, the values of parameters A, B and C in Eq. (3) can be found in Harvey's study (Harvey 1996). The partial molar volume of each component is obtained by temperature-dependent correlation (Computer Modelling Group 2012). The Harvey's correlation has demonstrated its ability to successfully fit with available data and even to extrapolate data to higher temperatures. Its mean standard deviation can be as low as 0.0087 and it is applicable over large temperature ranges (Harvey 1996). Furthermore, in order to consider the salting-out effects, the salting-out coefficient as a function of temperature is also adopted for each component to obtain the corresponding Henry's constant in brine (Computer Modelling Group, 2012).

As an example to illustrate the impact of gas composition on solubility, Figure 2 shows the solubility of CO_2 in different binary mixtures with impurity mole fraction up to 0.6 at fixed temperature 61 °C and pressure 110 bar with the salinity of 118950 mg/L. The solubility of H_2S is also shown while both the solubility of CH_4 and N_2 under the chosen conditions is lower than 1×10^{-4} and is thus neglected in the figure. It can be seen that when the impurity concentration is no more than 0.1, the solubility of CO_2 in different binary mixtures is similar. When the impurity concentration increases, however, the reduction of CO_2 solubility by different non-CO_2 species is slightly different. Compared with the gradual decrease of CO_2 solubility, H_2S solubility increases significantly with its increasing concentration in the CO_2-H_2S mixture because of its preferential solubility.

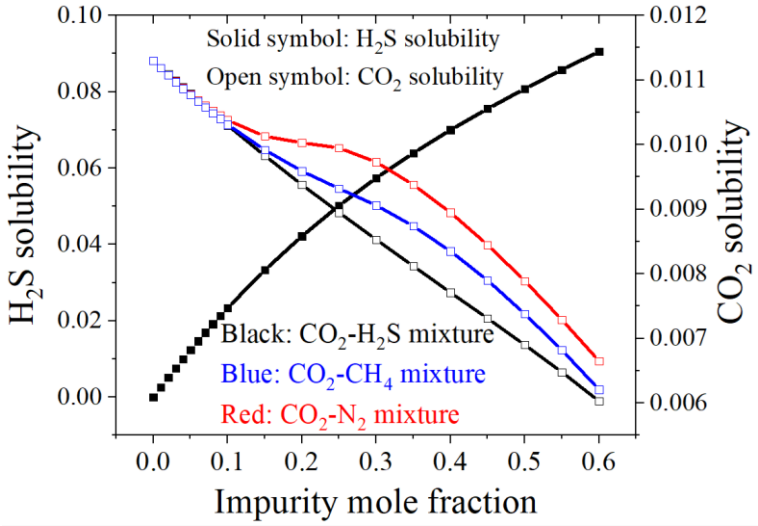

Figure 2 Solubility of CO_2 and H_2S in different binary mixtures at temperature 61 °C and pressure 110 bar with the salinity of 118950 mg/L.

The capillary pressure p_c is provided by the van Genuchten correlation (van Genuchten 1980) as follows,

$$p_c = -P_0\left(\left[S^*\right]^{-1/\lambda} - 1\right)^{1-\lambda} \tag{5}$$

$$S^* = \frac{S_l - S_{lr}}{1 - S_{lr}} \tag{6}$$

where P_0 is the strength coefficient which is 3.58×10^3 Pa for sand 62.0×10^3 Pa for shale, while the exponent λ is set as 0.4 (Pruess et al. 2002). S_l and S_{lr} represent the saturation of the liquid (aqueous) phase and the irreducible liquid saturation, respectively. The cutoff value of p_c is set as 10^7 Pa. The relative permeability of the aqueous phase is also described by the van Genuchten function (van Genuchten 1980) while that of the gaseous phase is computed by the Corey correlation (Corey 1954). The density and viscosity of the aqueous phase is obtained using the Rowe and Chou (Rowe and Chou 1970) correlation and Kestin et al. (Kestin et al. 1981) correlation respectively, while the density and viscosity of the gaseous phase are calculated by the Peng-Robinson EOS and the Lee-Eakin formula (Lee and Eakin 1964) respectively.

The Cartesian grid is used to discretize the present 2D model, consisting of 113 columns and 136 layers, while the one-meter width is represented by one grid block. Both the vertical and horizontal grid sizes near the injection point are as small as 0.25 m to capture the plume behavior of the injected streams. Apart from the injection point, significant gradients are also expected to occur near the shale layers. Therefore, a small vertical gridding of 0.75 m is implemented in the shale layers as well as the sands above and below them. Lower vertical resolution up to 3 m is adopted away from the injection point and the shale layers. Considering that the horizontal size of the model is 6000 m, the horizontal grid spacing away from the left boundary gradually increases to 125 m to achieve better computational efficiency. A very small grid size of 0.001 m is employed at the right boundary to implement the constant-hydrostatic-pressure profile. Furthermore, grid independence analysis in previous investigation using similar grid discretization without pre-dissolved impurities (Li et al. 2018) implies that the selected gird resolution is adequate to obtain reasonable results.

3. Results and discussions

3.1 Pressure profile

Pressure in the reservoir is expected to increase in response to the gas injection. Figure 3a demonstrates the pressure evolution at the injection well where it is expected to experience

significant pressure build-up. The general patterns for all the five scenarios are similar, *i.e.*, the pressure at the injection point increases rapidly due to the injection at the early stage and then gradually decreases during the rest of the injection period. Once the injection has stopped, the pressure decreases sharply. The pressure profiles in the whole field for the five scenarios are also similar and thus only the pressure profile for the 10% N_2 scenario is illustrated as an example (Figure 3b-d). As expected, the pressure buildup around the injection well is distinctly higher than the rest of the domain. In addition, the shale layers are implied to have an influence in the pressure propagation and distribution, *e.g.*, there are sharp edges in the pressure contour in shale layer SL1 in Figure 3b. After the injection has stopped for only one year, the pressure profile in the domain has almost reduced to the hydrostatic one.

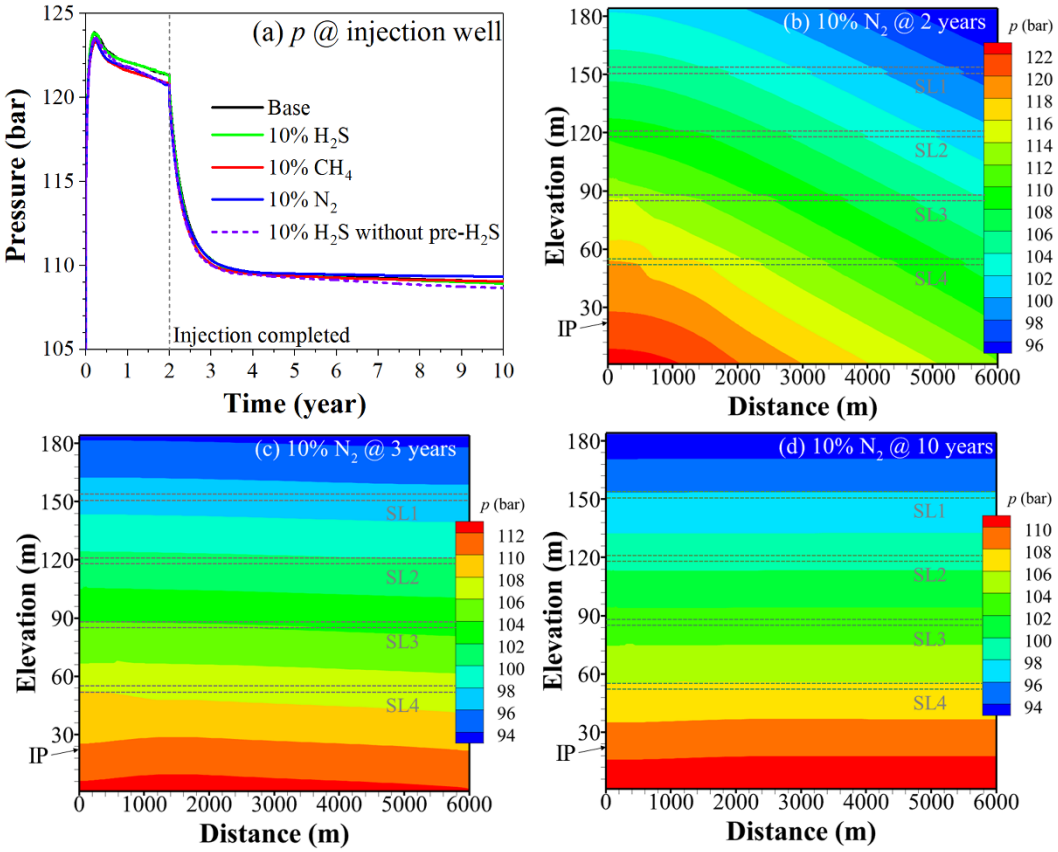

Figure 3 Pressure profile. (a) Pressure evolution at the injection well for all the scenarios, and (b)-(d) pressure profile for the 10% N_2 scenario at 2, 3, and 10 years respectively. The 3-meter shale layers (SL) embedded in the sand layers are manifested by the short dashed lines with their respective names shown beneath them. The following figures inherit the meaning of the short dashed lines presented here.

214 *3.2 Plume profile*

215 As shown in Figure 4, the plume footprint (S_g represents the fraction of pore volume occupied
216 by the gas phase) is used to track the position of the displacement front. For all the five scenarios,
217 the injected plume mainly distributes under the low-permeability shale layers SL3 and SL4 after 2
218 years injection. There is only a very small portion of the CO_2 stream that has penetrated up through
219 SL3 and spreading in the sand formation under SL2. To be more specific, the higher gas saturation
220 (S_g>0.5) mainly distributes in the sand layers immediately under SL3 and SL4 while the gas
221 saturation in the shale layers is much smaller.

222 Comparing the four scenarios injected into the sour (H_2S-saturated) aquifers with that into the
223 regular (H_2S-free) aquifer (Figure 4a-d vs. Figure 4e), it is obvious that the plume edges in the sour
224 saline aquifers are much oscillated. As for the four scenarios with different injected compositions
225 in the sour aquifers, the co-injection of 10% H_2S weakens the uprising of the leading plume to a
226 certain degree, partially due to the fact that the density of the H_2S impurity is over twice higher
227 than that of CO_2 under the reservoir conditions (Table 3), thus reducing the buoyance force of the
228 uprising plume. Besides, the plume mobility which is inversely proportional to phase viscosity
229 would decrease with the high-viscosity H_2S. The effects of co-injected impurity on the plume
230 mobility are more significant in terms of the horizontal migration. Since the viscosity of the non-
231 condensable gas impurities, *i.e.*, CH_4 and N_2, is smaller than that of CO_2, the leading edge of the
232 plume under SL4 is distinctly longer in the 10% CH_4 and 10% N_2 scenarios than in the other two
233 scenarios. The area with higher gas saturation (S_g>0.5) in these two scenarios is also relatively
234 larger. Despite the differences in the properties of CH_4 and N_2, including density, viscosity, and
235 solubility, the overall plume footprint in the 10% CH_4 and 10% N_2 scenarios is comparable.

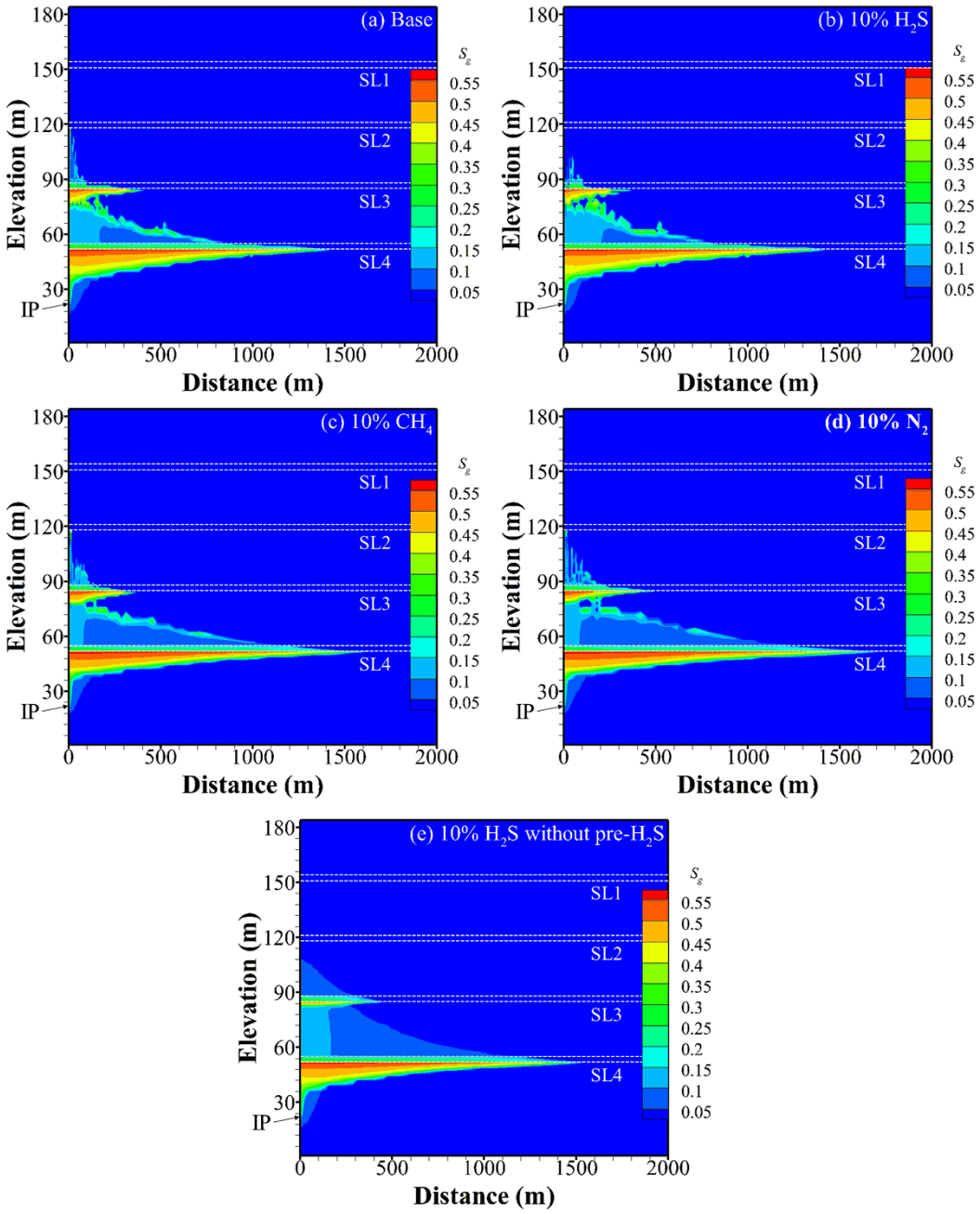

Figure 4. Plume footprint of different scenarios after 2 years injection.

Figure 5 shows the plume distribuiton after 10 years, inlcuding the 2 years injection and 8 years post-injection periods. The irregular plume edges observed in Figure 4a-d are smoothened to a certain degree after 10 years. The majority of the mobile plume accumulates immediately under the low-permeability shale layers SL3 and SL4 as a thin and horizontal layer while there is nearly no mobile gas left in the low-permeability shale layers. It can be seen that there is a small portion

of the plume starting to accumulate and spread under SL2 after 10 years, except for the 10% H_2S scenario in which the plume has not yet reached the shale layer SL2. In other words, the plume still could not penetrate through the shale layer SL2 even after 8 years post-injection period, partially because the pressure buildup caused by the gas injection rapidly decreases when the injection stops (Figure 3) while the buoyance force is not strong enough to overcome the capillary force of the shale layer with gases continueously dissolving into the formation brine.

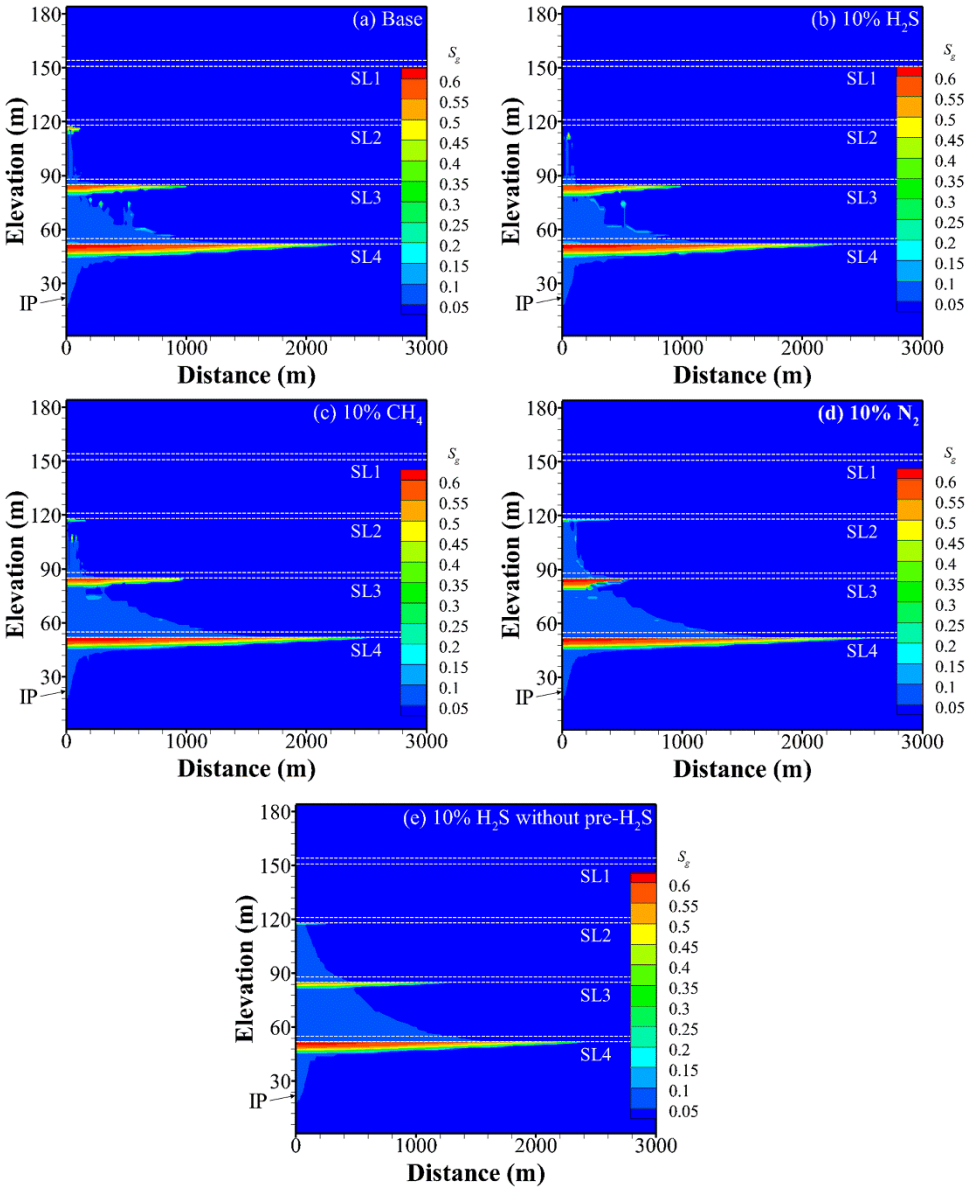

Figure 5. Plume footprint of different scenarios after 10 years.

3.3 Phase compositions

The compositions of different species in the plume after 2 years injection are shown in Figures 6-8 while Figure 9 shows the corresponding dissolved H_2S concentration in the formation brine. It should also be noted that in the upper half of the sour aquifer, the saturated H_2S concentration is slightly lower (Figure 9), which is because of the geothermal gradient and hydrostatic pressure gradient adopted in the model and thus the relatively lower temperature and pressure in the shallower section. Comparing the sour saline aquifers and the regular saline aquifers (*e.g.*, Figure 6a-d vs. Figure 6e), there are distinct differences in the patterns of the phase compositions. Specifically, if native H_2S is absent in the aquifer, CO_2 dominates in the leading plume ($\geq$0.9) while it has slightly lower concentration around the injection well (Figure 6e). In the meantime, H_2S concentration at the leading plume is rather low mainly due to its preferential solubility (Figure 7e). In addition, H_2S concentration in the plume could not exceed its concentration in the injected stream (0.1). In the sour saline aquifer, however, higher CO_2 concentration mainly distributes in the rear part of the plume (Figure 6a-d), while the H_2S mole fraction in the leading plume is generally higher than 0.1 because of the exsolved H_2S out of the aquifers (Figure 7a-d).

In the sour saline aquifers, the region swept by the plume can be divided into two sub-regions according to phase compositions. First, these is an inner sub-region that extends from the injection well in which the plume is determined by the injected gas compositions (Figure 6 and Figure 8). Except for the 10% H_2S scenario where H_2S is co-injected (Figure 7b), H_2S is almost absent in this inner sub-region. In fact, closer examination of scenarios a, c, and d in the inner sub-region reveals that the dominant mole fraction of H_2S in the plume and in the aqueous phase is lower than 0.001 (Figure 7a, c, and d) and 0.0001 (Figure 9a-d) respectively. This is mainly because that the gas injection has exsolved the pre-dissolved H_2S out of the formation brine and pushed it outwards. Second, there is an outer sub-region that extends from the outer edge of the inner sub-region to the two-phase interface. The plume composition in the outer sub-region is more complex than in the inner sub-region. Generally, the plume is still dominated by CO_2, especially in the parts near the inner sub-region (Figure 6). H_2S concentration in the plume gradually increases towards the leading

edge of the outer sub-region and reaches a peak value (Figure 7a-d). Particularly, when 10% CH_4 or N_2 is co-injected into the sour aquifers, the peak concentration of H_2S in the leading plume could even exceed 0.5 (Figure 7c and d), *i.e.*, the leading plume might be dominated by H_2S in some particular scenarios, while the concentration of CH_4 or N_2 in the leading plume is hardly over their corresponding mole fraction in the injected streams (Figure 8).

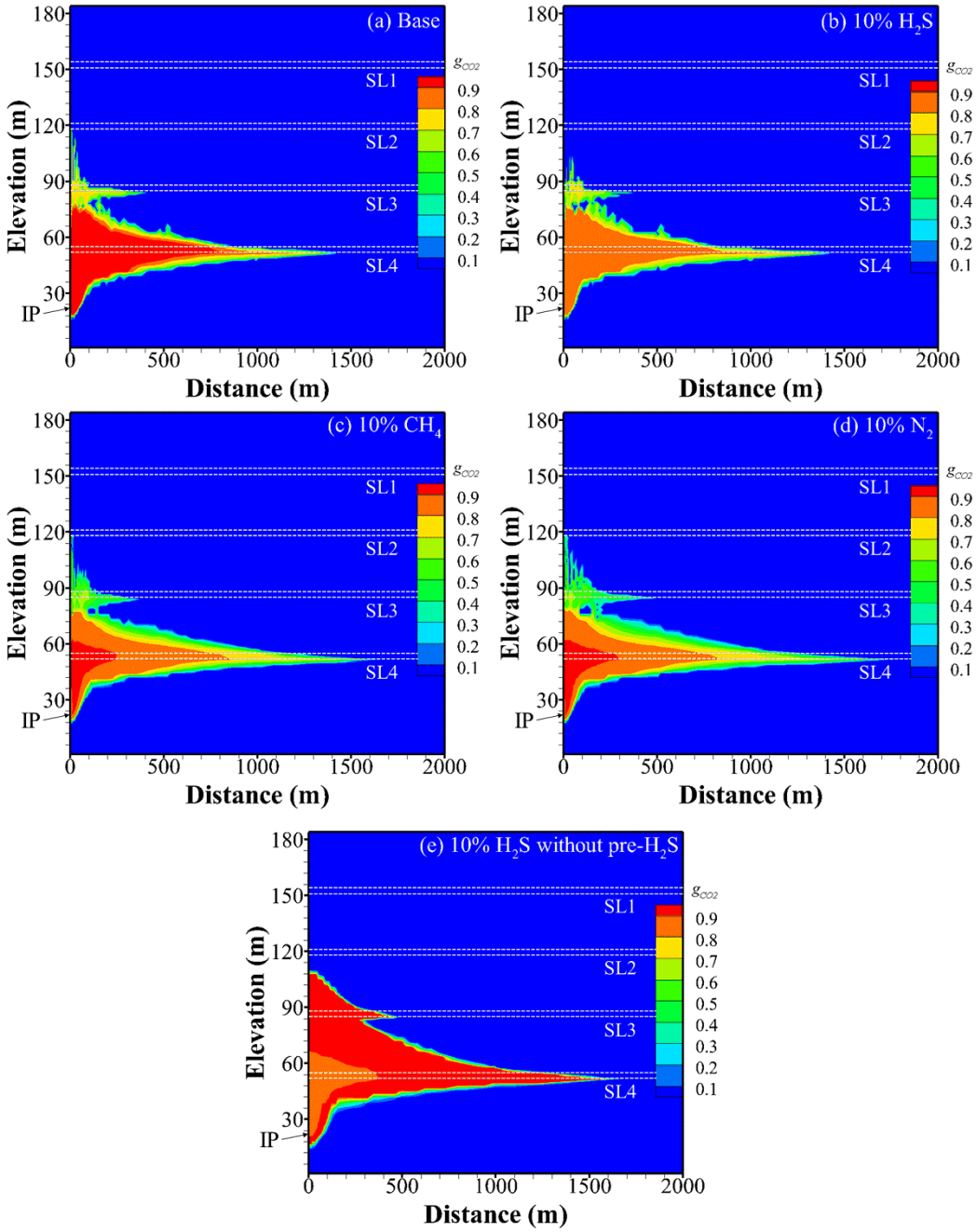

Figure 6. Mole fraction of CO_2 in the plume after 2 years injection for different scenarios.

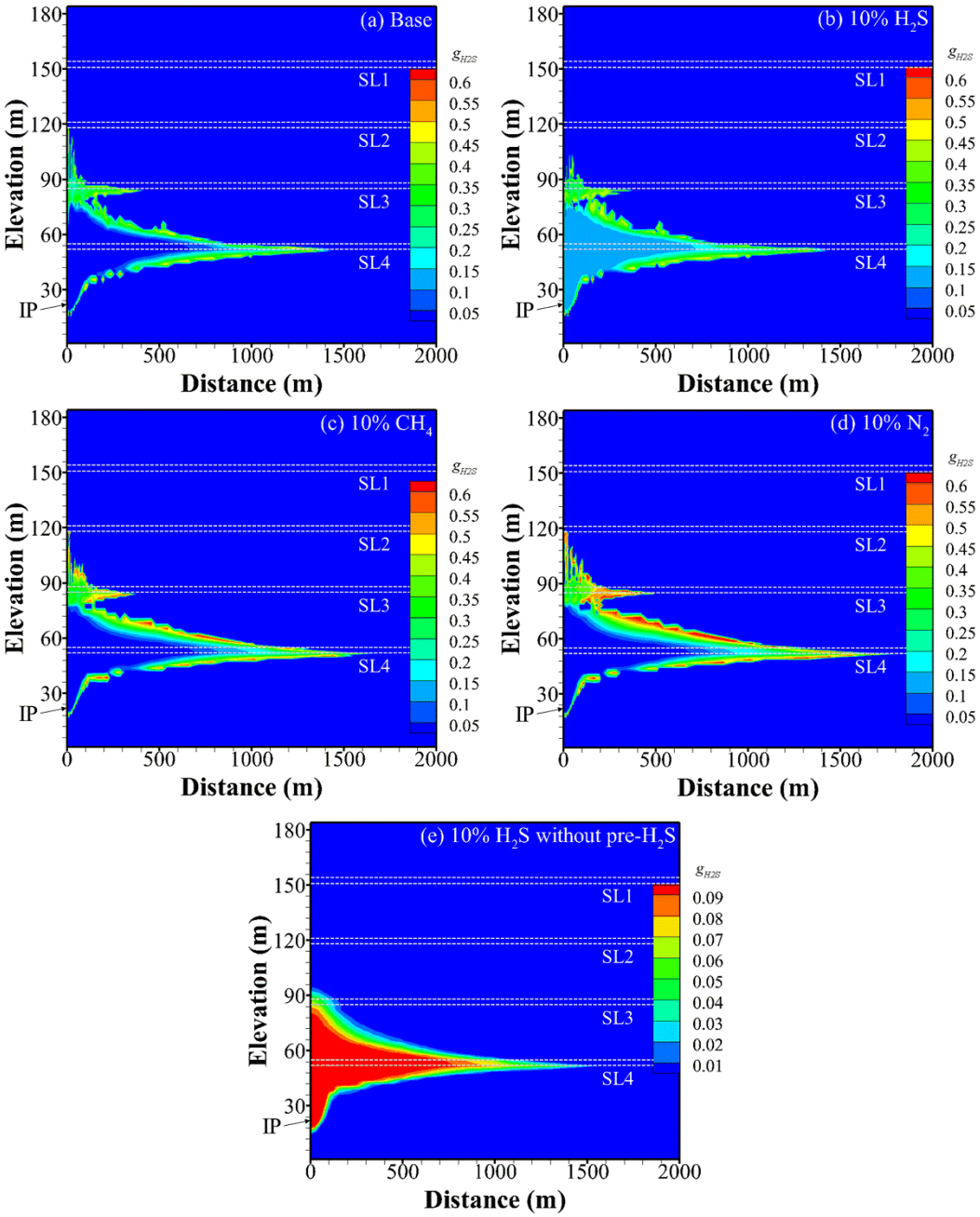

285

286 Figure 7. Mole fraction of H_2S in the plume after 2 years injection for different scenarios.

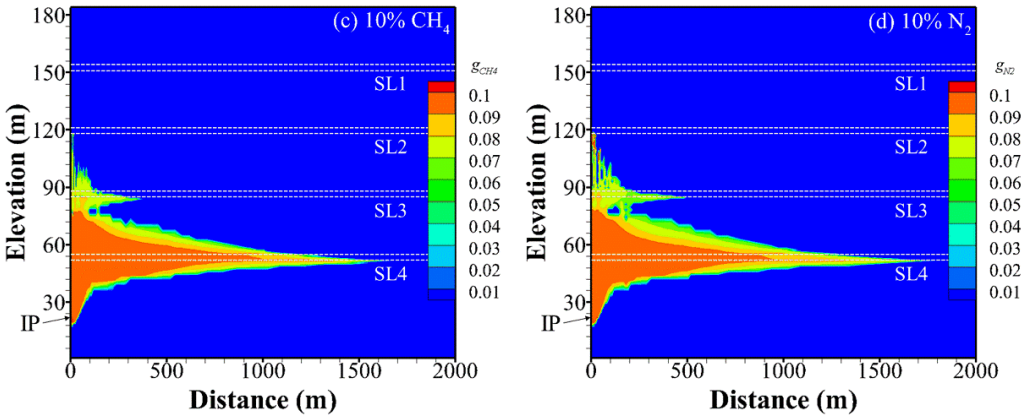

287

288 Figure 8. Mole fraction of co-injected non-condensable impurity in the plume after 2 years injection.

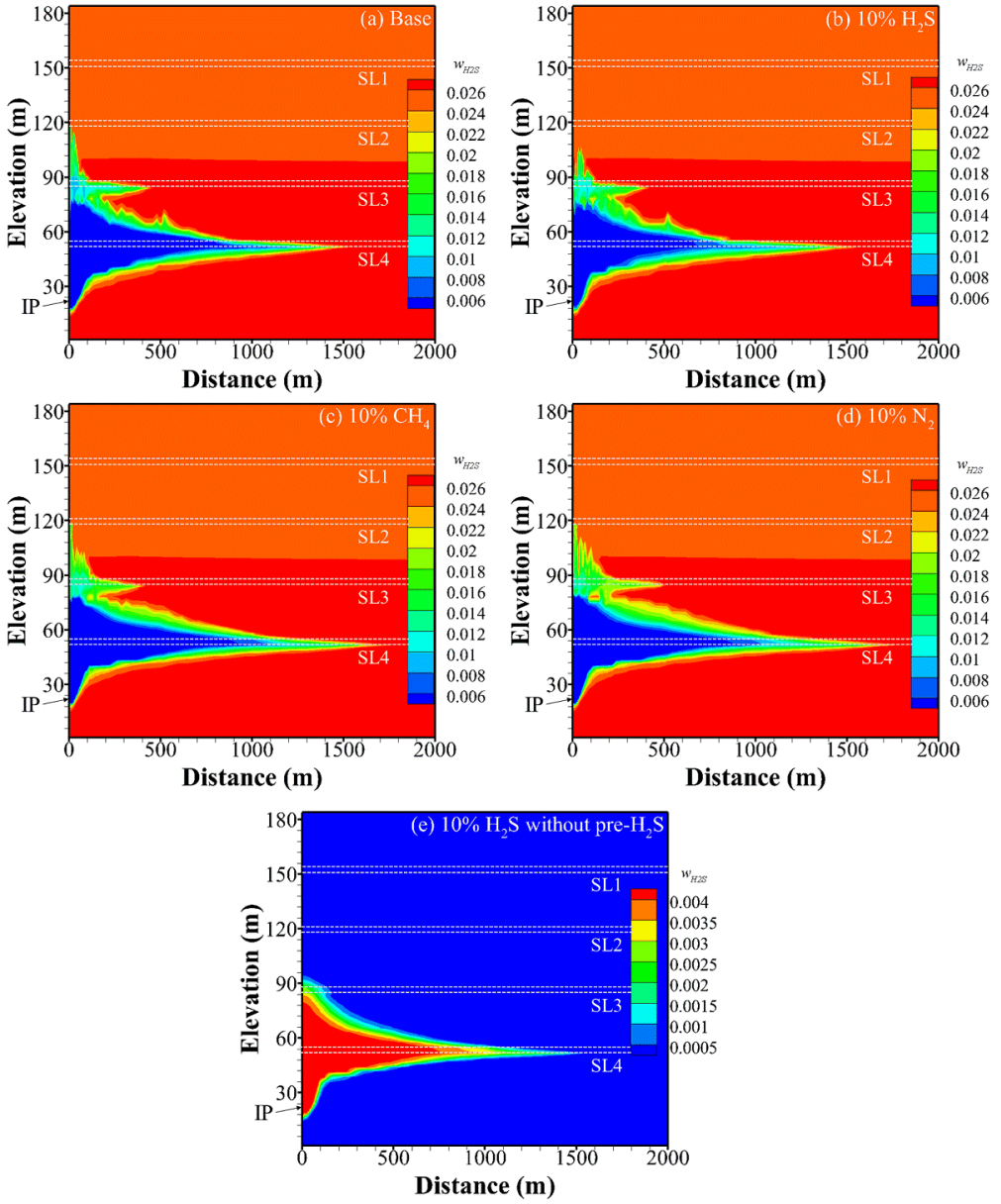

289

290 Figure 9. Dissolved H_2S mole fraction after 2 years injection for different scenarios.

3.4 CO_2 dissolution

Figure 10 shows the time evolution of the total injected CO_2 mass, supercritical CO_2 mass, dissolved CO_2 mass, and dissolved CO_2 fraction for different scenarios. For sour gas sequestration, the same amount of CO_2 is injected into the sour saline aquifer (10% H_2S) and the regular saline aquifer (10% H_2S without pre-H_2S) (Figure 10a). It can be seen that the existence of native H_2S results in much less dissolved CO_2 and thus more mobile CO_2. This may result from potential dissolution competition between H_2S (both exsolved and injected) and CO_2 in the sour saline aquifer and the smaller two-phase interface (Figure 4 and Figure 5). The pre-existing H_2S in the saline aquifers could be a strong competitor for potential CO_2 dissolution because of its preferential solubility in the formation brine. More importantly, the exsolved H_2S is often found ahead of the injected CO_2 plume in the outer sub-region (Figure 7), which makes the dissolution of CO_2 into the formation brine much harder. In fact, dissolved CO_2 fraction in the sour aquifers may be only half that in the corresponding scenario without native H_2S (Figure 10d). Moreover, the increase rate of the dissolved CO_2 fraction in the sour saline aquifer is also slower.

In the sour saline aquifers, the inclusion of different impurities decreases the total injected CO_2 mass to different degrees, with the largest reduction in the 10% N_2 scenario and the least redution in the 10% H_2S scenario (Figure 10a). Both the supercritical and dissolved CO_2 mass increases linearly with time during the injection period. After the injection stops, the supercritical CO_2 mass decreases gradually while both the dissolved CO_2 mass and fraction increase accordingly. The inclusion of all the co-injected impurities is expected to reduce the dissolved CO_2 mass. However, the inclusion of the N_2 and CH_4 impurity could increase the dissolved CO_2 ratio compared with the pure CO_2 scenario. Still, even for the 10% N_2 scenario, CO_2 dissolution fraction is distinctively lower than in the 10% H_2S scenario without native H_2S in the saline aquiers.

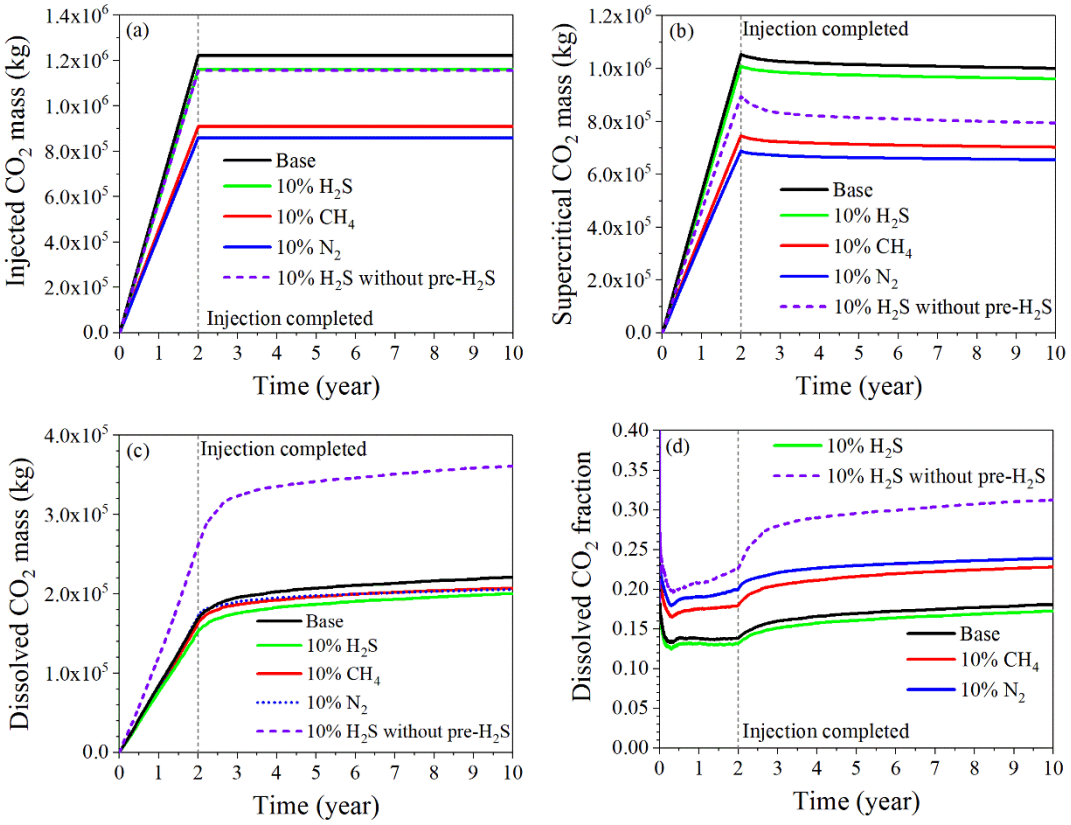

Figure 10. Evolution of (a) total injected CO_2 mass, (b) supercritical CO_2 mass, (c) dissolved CO_2 mass, and (d) dissolved CO_2 fraction for different scenarios during 10 years.

3.5 Long-term evaluation

The time scale in practical CO_2 sequestration projects is generally up to hundreds to thousands of years. To evaluate the long-term fate of the plume spread and the dissolved CO_2 in the deep saline aquifers, the simulation time in this subsection has been extended to 100 years, including 2 years injection and 98 years post-injection periods. As shown in Figure 11, even after an extra 90 years, the plume is still not able to penetrate through the shale layer SL2 and the plume profile for different scenarios seems similar after 10 years (Figure 5). However, the plume saturation reduces (Figure 11) and the dissolved CO_2 inventory increases (Figure 12) with the extended plume migration and the continuous dissolution of CO_2 in the aqueous phase.

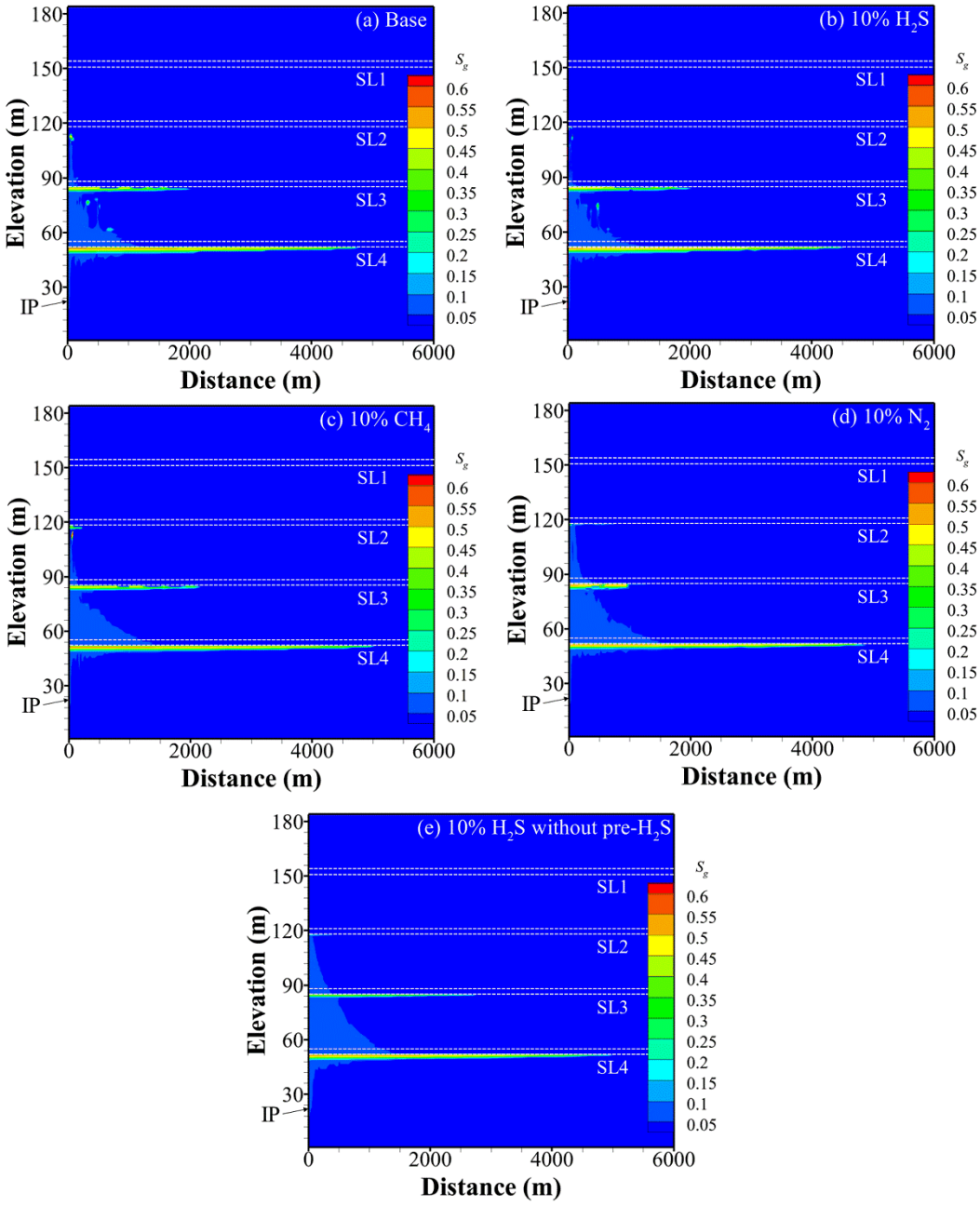

Figure 11. Plume footprint of different scenarios after 100 years.

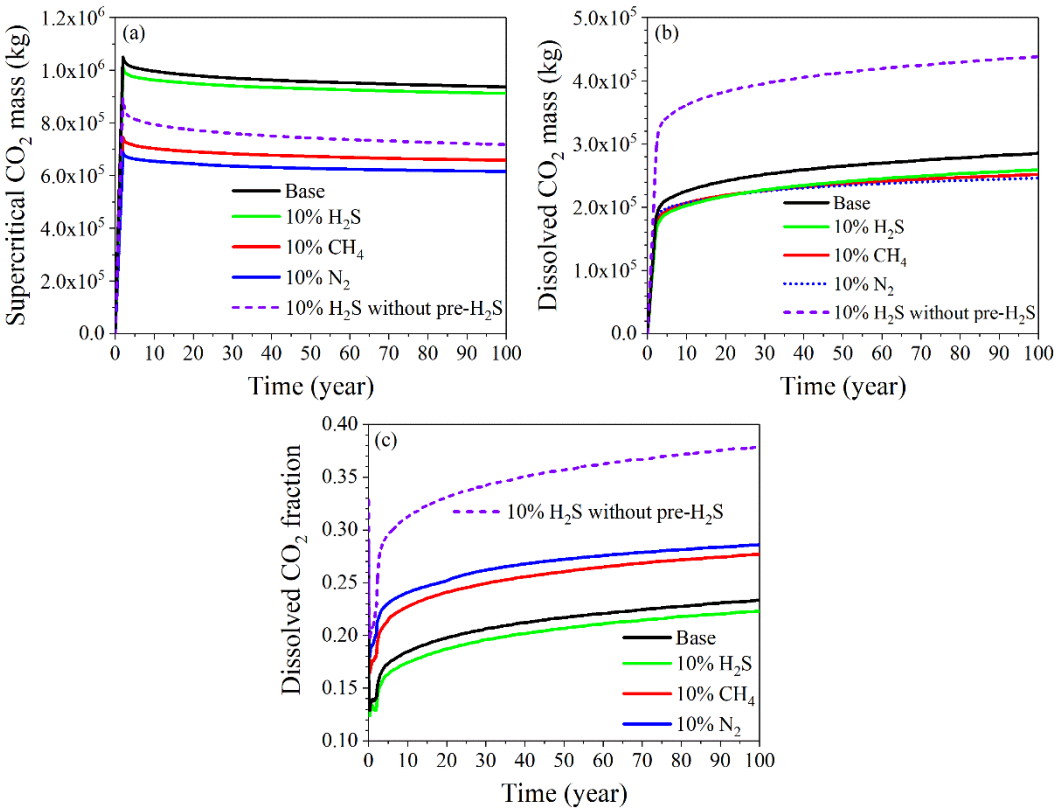

Figure 12. Evolution of (a) supercritical CO_2 mass, (b) dissolved CO_2 mass, and (c) dissolved CO_2 fraction for different scenarios during 100 years.

In the sour aquifers, the profile of H_2S concentration in the plume (Figure 13) is used to illustrate the coupling effects of different co-injected impurities and the native H_2S on the development of the advancing plume footprint as well as the evolution of the inner and outer sub-regions as mentioned above. There is no definite boundaries between these two sub-regions which are more of a theoretical conception than a quantification. In the present study, two levels of contour lines (0.05, 0.15) of H_2S mole fraction in the plume are selected to separate the inner and outer sub-regions for the 10% H_2S scenario (Figure 13b) while one level (0.05) is enough for all the other scenarios. Generally speaking, the distribution area of the plume increases with time, especially in the horizontal direction. In the vertical direction, the plume migrates upwards gradually while the migration is much affected by the low-permeable shale layers. Comparing the area covered by the innermost red contour line (2 years), the innermost black contour line (10 years), and the innermost blue contour line (100 years), it can be seen that the area of the inner sub-region increases

indistinctively with time or injection compositions. Closer examination shows that the horizontal distance of the inner sub-region increases with time while its bottom contour migrates slightly upwards. In contrast, the outer sub-region in the 10% CH_4 and 10% N_2 scenarios is much extended with time, especially in the horizontal direction of the 10% N_2 scenario.

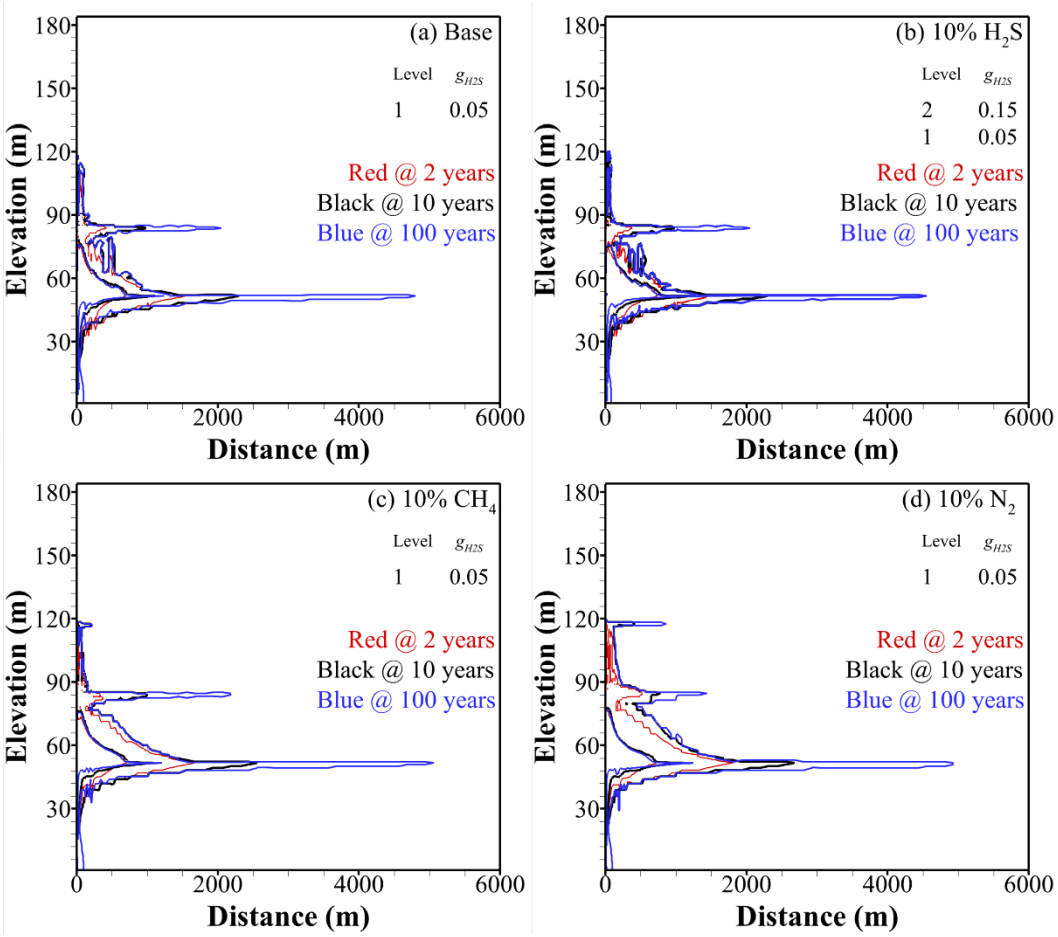

Figure 13. Development of plume edges as well as the inner and outer sub-regions for different scenarios in the sour saline aquifers.

Figure 14 further illustrates the evolution of the horizontal plume migration for different scenarios in the sour saline aquifers and Table 4 compares their mean migration rate during different time periods. Generally speaking, the migration rate in the post-injection period is distinctively weakened because of the cessation of the injection. For example, the total horizontal migration distance of the advancing plume in the 8 years post-injection period is only approximately half of that in the 2 years injection period. The inclusion of the N_2 or CH_4 impurity is favorable for the

horizontal migration in the sour saline aquifers mainly due to their low viscosity and thus their positive effects on the plume mobility. During the injection period, the mean migration rate of the 10% CH_4 or N_2 scenario is distinctively higher than that of the other two scenarios. After the injection stops, however, the differences of the mean migration rate between different scenarios are insignificant and mainly depend on the plume compositions and properties. For instance, the exsolved H_2S with high concentration ahead of the injected plume might reduce the potential enhancement of the more mobile and buoyant CH_4 or N_2 on the plume migration. Because of the pressure buildup caused by the injection (Figure 3), the mean migration rate during the early stage of the post-injection (*i.e.*, 3-10 years) is higher than that during the late one (*i.e.*, 11-100 years). Above all, there is no significant differences in the mean migration rate between the plumes with different compositions during the post-injection period.

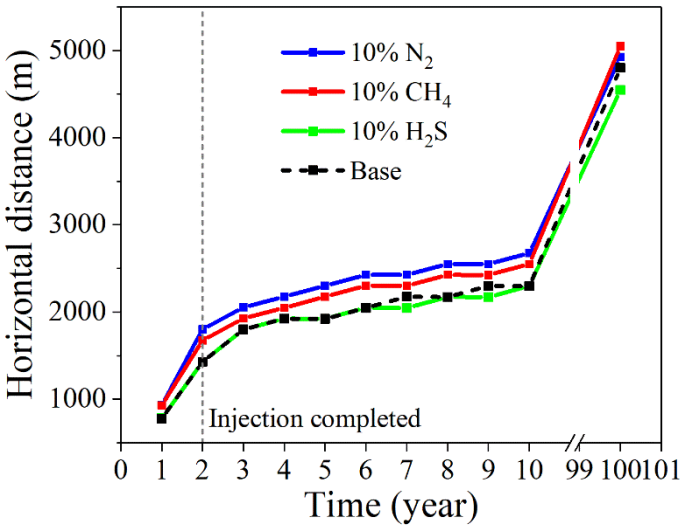

Figure 14. Evolution of horizontal migration distance for different scenarios in the sour saline aquifers.

Table 4. Mean migration rate in the horizontal direction during different time periods.

Scenario	0-2 years (m/yr)	3-10 years (m/yr)	11-100 years (m/yr)
Base	714.64	108.51	27.80
10% H_2S	714.60	108.73	24.98
10% CH_4	836.92	109.73	27.76
10% N_2	901.18	109.22	25.00

3.6 Discussions

Some potential reservoirs for CO_2 sequestration may contain pre-existing species and the sour saline aquifers containing dissolved H_2S attracts our attention due to the high toxicity of H_2S. According to the one-dimensional numerical and analytical simulation results in the previous studies (Cholewinski et al. 2016, Ghaderi et al. 2011a, b), gas injection would exsolve the native H_2S out of the aqueous phase and the exsolved H_2S would then be pushed outwards along with the formation brine by the injecting CO_2 plume. On the other hand, most practical carbon sequestration projects involve co-injected impurities, and the injected gases are expected to dissolve into the formation brine at the two-phase interface. Particularly, in regular aquifers without native H_2S, the partitioning phenomenon of different co-injected gas species is likely to occur at the two-phase interface, leaving low-solubility and low-viscosity species such as N_2 or CH_4 as the dominant ones in the leading plume while the co-injected H_2S would be stripped off at the leading plume because of its preferential solubility (Li et al. 2017, 2018). Therefore, when both the co-injected and the native impurities exist, their coupling effects on CO_2 sequestration should be evaluated in order to obtain a better understanding of impure CO_2 storage.

To begin with, the plume edges in the sour aquifers are observed to have distinct oscillations in comparison with that in the H_2S-free aquifers, especially during the injection period. When CO_2 and/or non-CO_2 species are injected, the reservoir conditions such as pressure change rapidly and the plume continuously displaces the formation brine. It is suggested that all the relevant species simultaneously seek to attain equilibrium at the advancing two-phase boundary, including the exsolution and/or dissolution of the native H_2S, and the dissolution competition between the injected components. Above all, the leading plume experiences rapid and continuous changes during the injection period, which might be the reason for the oscillated plume edges. After the injection stops, the migration of the leading plume weakens distinctively and thus the oscillation of the plume edges would become smoothened (*e.g.*, Figure 4 vs. Figure 5). Since the plume patterns and the phase compositions at the two-phase interface play an important role in the plume migration, the potential dissolution and thus the security of the long-term CO_2 sequestration, further

experiments are needed to confirm these predictions.

While the partitioning phenomenon of different injected species is not obvious at the leading plume, our results in the stratified formation confirm the exsolution of the pre-existing H_2S and the generation of two distinguishable sub-regions in the plume (Ghaderi et al. 2011a). In the inner sub-region, the native H_2S is almost removed out of the brine, *i.e.*, plume compositions in the inner sub-region are generally determined by the injection stream. In the outer sub-region, on the other hand, the exsolved H_2S concentration gradually increases towards the leading plume edge, which might exceed 50% depending on the reservoir conditions. Since the potential dissolution mainly happens at the two-phase interface, the existence of the outer sub-region especially the high-solubility exsolvd H_2S with high-concentration is not favorable for the dissolution of the injected gases including CO_2. Actually, the native H_2S has negative effects on both CO_2 dissolution inventory and ratio, especially when H_2S is co-injected with CO_2. However, when less soluble impurities such as CH_4 or N_2 are co-injected into the sour saline aquifers, CO_2 dissolution ratio would be enhanced. It should be noted here that while the dissolution of CO_2 may not increase the storage capacity, it is expected to increase the storage security (Bachu 2008, Metz et al. 2005). In addition, CO_2 dissolution provides the preconditions of geochemical reactions that could converse dissolved CO_2 into carbonate minerals. This discussion does not suggest that the dissolution trapping mechanism is more secure than the static trapping mechanism of mobile and buoyant CO_2 in stratigraphic and structural traps. It only implies that if the dissolution trapping mechanism increases its contribution, the storage security is expected to increase in time (Bachu 2008).

In general, compared with the co-injected impurities, the native impurity like H_2S seems to have more profound effects on CO_2 sequestration in the saline aquifers. The present study could provide references for CO_2 sequestration in the sour saline aquifers. For example, the reservoirs with native H_2S may not be ideal sequestration sites for sour gas disposal involving H_2S. Although the co-injection of CH_4 or N_2 decrease CO_2 storage capacity and may relatively increase the leakage risk because of the extended plume spread, the dissolution CO_2 ratio increases significantly compared with the pure CO_2 injection. Besides, the increase of the plume migration rate is

insignificant after the injection has stopped. On the other hand, the formation and evolution of two sub-regions in the plume could also be useful for making monitoring management plans. These results should be considered in the selection of suitable sequestration site and the determination for the injection plans of impure CO_2 injection in the sour saline aquifers.

4. Conclusions and future work

In the present study, the coupling effects of the native H_2S and different co-injected non-CO_2 species on CO_2 sequestration in layered saline aquifers were examined and compared. Apart from the more expected result that the low-permeability shale layers could affect the pressure propagation and particularly the plume migration and distribution, our simulation results and discussions about the coupling effects of the co-injected and native impurities suggest that:

1) There is an obvious oscillation in the plume edges when the CO_2 streams are injected into the sour aquifers containing native H_2S, which is much alleviated after the injection has stopped.

2) The plume could be divided into two sub-regions according to the phase compositions while the existence of the outer sub-region with high concentration of exsolved H_2S is negative to CO_2 dissolution.

3) The co-injection of less soluble impurities such as N_2 or CH_4 into the sour aquifers could increase CO_2 dissolution ratio. In addition, these two impurities could enhance the plume spread during the injection period, while there is an insignificant difference in the plume migration pattern or rate between different scenarios during the post-injection period.

4) Compared with the co-injected impurities, the native impurities such as H_2S are expected to have more profound impact on CO_2 dissolution and thus the security and permanency of CO_2 sequestration.

The simulations in this study are limited by the simplification of the 2D model and the thermodynamic and transport models. For example, the molecular diffusion which affects both the plume spread and the back-mixing mechanism is neglected. In future work, the effects of the

diffusivity of different species on the plume alternation will be investigated. In addition, the details of the permeability structure including reservoir heterogeneity, the angle of the layers, and the multi-injection scheme which are practically relevant in the stratified formations should also be taken into account.

Acknowledgement

This work was supported by the National Natural Science Foundation of China (Grant No. 41807191) and the Natural Science Foundation of Guangdong Province, China (Grant No. 2018A030310524). We also appreciated the One Hundred Young Talents Program of Guangdong University of Technology for its financial support (1143-220413560). We also would like to thank the anonymous reviewers for their insightful comments, as they have led to a great improvement of the work.

References

Aminu, M.D., Nabavi, S.A., Rochelle, C.A. and Manovic, V. (2017) A review of developments in carbon dioxide storage. Applied Energy 208, 1389-1419.

Bachu, S. (2008) CO_2 storage in geological media: Role, means, status and barriers to deployment. Progress in Energy and Combustion Science 34(2), 254-273.

Battistelli, A. and Marcolini, M. (2009) TMGAS: A new TOUGH2 EOS module for the numerical simulation of gas mixtures injection in geological structures. International Journal of Greenhouse Gas Control 3(4), 481-493.

Celia, M.A. (2017) Geological storage of captured carbon dioxide as a large-scale carbon mitigation option. Water Resources Research 53(5), 3527-3533.

Cholewinski, A., Dengis, J., Malkov, V. and Leonenko, Y. (2016) Modeling of CO_2 injection into aquifers containing dissolved H_2S. Journal of Natural Gas Science and Engineering 36, 1080-1086.

Computer Modelling Group (CMG).(2012) User's Guide-GEM: Advanced compositional and unconventional reservoir simulator. Version 2012. Computer Modelling Group Ltd., Calgary, AB, Canada.

Corey, A.T. 1954. The interrelation between gas and oil relative permeabilities. Producers Monthly 19(1), 38–41.

Doughty, C. and Freifeld, B.M. (2013) Modeling CO_2 injection at Cranfield, Mississippi: Investigation of methane and temperature effects. Greenhouse Gases-Science and Technology 3(6), 475-490.

Ganjdanesh, R., Pope, G.A. and Sepehrnoori, K. (2015) Production of energy from saline aquifers: A method to offset the energy cost of carbon capture and storage. International Journal of Greenhouse Gas Control 34, 97-105.

Ghaderi, S.M., Keith, D.W., Lavoie, R. and Leonenko, Y. (2011a) Evolution of hydrogen sulfide in sour saline aquifers during carbon dioxide sequestration. International Journal of Greenhouse Gas Control 5(2), 347-355.

Ghaderi, S.M., Keith, D.W., Lavoie, R. and Leonenko, Y. (2011b) Risk associated with H_2S evolution in sour aquifers during CO_2 injection. Energy Procedia 4, 4117–4123.

Ghaderi, S.M. and Leonenko, Y. (2015) Reservoir modeling for Wabamun lake sequestration project. Energy Science & Engineering 3(2), 98-114.

Harvey, A.H. (1996) Semiempirical correlation for Henry's constants over large temperature ranges. AIChE Journal 42(5), 1491–1494.

Hosseini, S.A., Mathias, S.A. and Javadpour, F. (2012) Analytical Model for CO_2 Injection into Brine Aquifers-Containing Residual CH_4. Transport in Porous Media 94(3), 795-815.

Hovorka, S.D., Meckel, T.A., Trevino, R.H., Lu, J., Nicot, J.-P., Choi, J.-W., Freeman, D., Cook, P., Daley, T.M., Ajo-Franklin, J.B., Freifeild, B.M., Doughty, C., Carrigan, C.R., Brecque, D.L., Kharaka, Y.K., Thordsen, J.J., Phelps, T.J., Yang, C., Romanak, K.D., Zhang, T., Holt, R.M., Lindler, J.S. and Butsch, R.J. (2011) Monitoring a large volume CO_2 injection: Year two results from SECARB project at Denbury's Cranfield, Mississippi, USA. Energy Procedia 4, 3478-3485.

Hutcheon, I. (1999) Controls on the distribution of non-hydrocarbon gases in the Alberta Basin. Bulletin of Canadian Petroleum Geology 47(4), 573-593.

Jiang, X. (2011) A review of physical modelling and numerical simulation of long-term geological storage of CO_2. Applied Energy 88(11), 3557-3566.

Kestin, J., Khalifa, H.E., Correia, R.J. (1981) Tables of the dynamic and kinematic viscosity of aqueous NaCl solutions in the temperature range 20–150 °C and pressure range 0.1–35 MPa. Journal of Physical and Chemical Reference Data 10, 71–87.

Lee, A.L. and Eakin, B.E. (1964) Gas-phase viscosity of hydrocarbon mixtures. Society of Petroleum Engineers Journal 4(3), 247-249.

Li, D., He, Y., Zhang, H., Xu, W. and Jiang, X. (2017) A numerical study of the impurity effects on CO_2 geological storage in layered formation. Applied Energy 199, 107-120.

Li, D., Zhang, H., Li, Y., Xu, W. and Jiang, X. (2018) Effects of N_2 and H_2S binary impurities on CO_2 geological storage in stratified formation – A sensitivity study. Applied Energy 229, 482-492.

Li, H., Jakobsen, J.P., Wilhelmsen, Ø. and Yan, J. (2011) PVTxy properties of CO_2 mixtures relevant for CO_2 capture, transport and storage: Review of available experimental data and theoretical models. Applied Energy 88, 3567-3579.

Li, J. and Li, X. (2015) Analysis of U-tube sampling data based on modeling of CO_2 injection into CH_4 saturated aquifers. Greenhouse Gases-Science and Technology 5(2), 152-168.

Li, Y., Nghiem, L.X. (1986) Phase equilibria of oil, gas and water/brine mixtures from a cubic equation of state and Henry's law. The Canadian Journal of Chemical Engineering 64(3), 486–496.

Metz, B., Davidson, O., de Coninck, H., Loos, M., Meyer, L.(2005) IPCC special report on carbon dioxide capture

514 and storage. Cambridge, United Kingdom and New York, USA: Cambridge University Press.

515 Oh, J., Kim, K.-Y., Han, W.S., Kim, M. and Park, E. (2019) Heterogeneity effects on pressure and CO_2 saturation
516 during core-scale multiphase flow tests. Journal of Petroleum Science and Engineering 172, 1174-1185.

517 Oldenburg, C.M., Doughty, C. and Spycher, N. (2013) The role of CO_2 in CH_4 exsolution from deep brine:
518 Implications for geologic carbon sequestration. Greenhouse Gases-Science and Technology 3(5), 359-377.

519 Pruess, K., García, J., Kovscek, T., Oldenburg, C., Rutqvist, J., Steefel, C., Xu, T. (2002) Intercomparison of
520 Numerical Simulation Codes for Geologic Disposal of CO_2, Lawrence Berkeley National Laboratory Report LBNL-
521 51813, Berkeley, CA 94720.

522 Pruess, K., García, J., Kovscek, T., Oldenburg, C., Rutqvist, J., Steefel, C., Xu, T. (2004) Code intercomparison
523 builds confidence in numerical simulation models for geologic disposal of CO_2. Energy 29(9-10), 1431–1444.

524 Qafoku, N.P., Lawter, A.R., Bacon, D.H., Zheng, L., Kyle, J. and Brown, C.F. (2017) Review of the impacts of
525 leaking CO_2 gas and brine on groundwater quality. Earth-Science Reviews 169, 69-84.

526 Rowe. A.M., Chou, J.C.S. (1970) Pressure-volume-temperature-concentration relation of aqueous NaCl solutions.
527 Journal of Chemical & Engineering Data 15, 61–66.

528 Soltanian, M.R., Amooie, M.A., Cole, D.R., Darrah, T.H., Graham, D.E., Pfiffner, S.M., Phelps, T.J. and Moortgat,
529 J. (2018) Impacts of methane on carbon dioxide storage in brine formations. Groundwater 56(2), 176-186.

530 Taggart, I. (2010) Extraction of dissolved methane in brines by CO_2 injection implication for CO_2 sequestration.
531 SPE 124630.

532 Talman, S. (2015) Subsurface geochemical fate and effects of impurities contained in a CO_2 stream injected into
533 a deep saline aquifer: What is known. International Journal of Greenhouse Gas Control 40, 267-291.

534 van Genuchten, M.Th. (1980) A closed-form equation for predicting the hydraulic conductivity of unsaturated
535 soils, Soil Science Society of America Journal 44, 892-898.

536 Zangeneh, H., Jamshidi, S. and Soltanieh, M. (2013) Coupled optimization of enhanced gas recovery and carbon
537 dioxide sequestration in natural gas reservoirs: Case study in a real gas field in the south of Iran. International Journal
538 of Greenhouse Gas Control 17, 515-522.